

Coupling-diversity-enhanced weak signal propagation in bistable networks

Yashi Zhang(章雅诗), Shanshan Cheng(程姗姗), Jie Fu(扶杰), and Lulu Lu(鹿露露)
Citation: Chin. Phys. B, 2026, 35 (**4**): 048704. DOI: 10.1088/1674-1056/ae23a9
http://cpb.iphy.ac.cn; http://iopscience.iop.org/cpb

What follows is a list of articles you may be interested in

A solution method for decomposing vector fields in Hamilton energy

Xin Zhao(赵昕), Ming Yi(易鸣), Zhou-Chao Wei(魏周超), Yuan Zhu(朱媛), and Lu-Lu Lu(鹿露露)
Chin. Phys. B, 2024, 33 (**9**): 098702. DOI: 10.1088/1674-1056/ad5a74

A progressive surrogate gradient learning for memristive spiking neural network

Shu Wang(王姝), Tao Chen(陈涛), Yu Gong(龚钰), Fan Sun(孙帆), Si-Yuan Shen(申思远), Shu-Kai Duan(段书凯), and Li-Dan Wang(王丽丹)
Chin. Phys. B, 2023, 32 (**6**): 068704. DOI: 10.1088/1674-1056/acb9f6

Simulation of the physical process of neural electromagnetic signal generation based on a simple but functional bionic Na^+ channel

Fan Wang(王帆), Jingjing Xu(徐晶晶), Yanbin Ge(葛彦斌), Shengyong Xu(许胜勇),Yanjun Fu(付琰军), Caiyu Shi(石蔡语), and Jianming Xue(薛建明)
Chin. Phys. B, 2022, 31 (**6**): 068701. DOI: 10.1088/1674-1056/ac3cac

Long range electromagnetic field nature of nerve signal propagation in myelinated axons

Qing-Wei Zhai(翟卿伟), Kelvin J A Ooi(黄健安), Sheng-Yong Xu(许胜勇), and C K Ong(翁宗经)
Chin. Phys. B, 2022, 31 (**3**): 038701. DOI: 10.1088/1674-1056/ac1e1a

Computational model investigating the effect of magnetic field on neural-astrocyte microcircuit

Li-Cong Li(李利聪), Jin Zhou(周瑾), Hong-Ji Sun(孙洪吉), Peng Xiong(熊鹏), Hong-Rui Wang(王洪瑞), Xiu-Ling Liu(刘秀玲), and Chang-Yong Wang(王常勇)
Chin. Phys. B, 2021, 30 (**6**): 068702. DOI: 10.1088/1674-1056/abea81

SPECIAL TOPIC — Biophysical circuits: Modeling & applications in neuroscience

Coupling-diversity-enhanced weak signal propagation in bistable networks

Yashi Zhang(章雅诗), Shanshan Cheng(程姗姗), Jie Fu(扶杰), and Lulu Lu(鹿露露)[†]

School of Mathematics and Physics, China University of Geosciences, Wuhan 430074, *China*

(Received 5 September 2025; revised manuscript received 24 November 2025; accepted manuscript online 25 November 2025)

Coupling diversity significantly shapes signal transmission and enhancement by modulating internal component interactions in nonlinear systems. Existing theoretical studies on coupling diversity have primarily focused on one-dimensional bistable systems, which are limited to single-variable scenarios and simple dynamical behaviors and thus fail to adapt to complex real-world systems or reveal multi-dimensional mechanisms. To address these limitations, the present study extends this investigation to two-dimensional globally coupled bistable systems. The research team explores the law of weak signal propagation in a globally coupled model composed of bistable oscillators, in which the coupling strength between oscillators follows a Gaussian distribution. Through dual verification via numerical simulations and analytical calculations, we confirm that when the coupling diversity is at an intermediate level, a resonance effect is induced within the system. This effect directly causes the system's dynamical properties to bifurcate into three oscillation clusters with significant differences. Such a bifurcation phenomenon can significantly amplify the system's collective response to weak external signals. Specifically, with an increase in the mean coupling strength, the peaks of the spectral amplification factor become higher, and the optimal variance exhibits a right-shifting trend. Notably, this phenomenon stably emerges across different system sizes, demonstrating the robustness of the system. This finding provides a reference for a deeper understanding of the regulatory mechanism of coupling diversity in weak signal propagation.

Keywords: coupling diversity, weak signal propagation, bistable oscillators, analytical calculations

PACS: 87.19.L–, 87.19.Lj, 05.45.–a, 05.45.Pq

DOI: 10.1088/1674-1056/ae23a9 **CSTR:** 32038.14.CPB.ae23a9

1. Introduction

The detection and enhancement of weak signals are important research topics in biological systems; for example, in the nervous system, high-frequency brain waves (20 kHz–50 MHz) generated by brain activity contain key information such as complex cognition and emotional regulation. However, these signals have low amplitude and are vulnerable to interference; their detection and enhancement help promote the development of brain–computer interface technology.[1] In the field of bioelectrical signal detection, human physiological electrical signals such as electroencephalographic (EEG) and electrocardiographic (ECG) signals have amplitudes only in the microvolt to millivolt range. Methods based on parameter-adjusted stochastic resonance can utilize the synergistic effects of noise, signals, and nonlinear systems to enhance these weak signals, aiding in early disease diagnosis.[2] For instance, in the detection of epileptic EEG signals, this technology can improve detection accuracy. In the cerebrospinal fluid of Alzheimer's disease patients, biomarkers such as tau protein and Aβ oligomers are present at extremely low concentrations (often below the picomolar level) and are easily interfered with by background noise. Enhancing such weak signals through surface-enhanced Raman spectroscopy (SERS) technology modified with nanomaterials enables ultra-early screening of the disease.[3]

Weak signals are often hidden in noise and are difficult to detect and recognize directly. Therefore, how to effectively extract and enhance these signals has become a key issue.[4–8] Stochastic resonance (SR), which is a unique phenomenon, offers new ideas and methods to solve this problem.[9–13] In stochastic resonance, appropriate noise can enhance the system's response to weak signals, thereby realizing the detection and enhancement of signals.[14–19]

In the case of global coupling, neurons form complex network structures through mutual connections and interactions, and this structure has an important influence on the propagation and processing of signals.[20–26] As the basic components of the nervous system, neurons rely on accurate perception of and responses to external stimuli to maintain their normal functioning.[27,28] In many biological systems, neurons interact with each other through complex network connections to form highly complex information-processing systems. Traditional studies mostly focus on uniformly coupled systems.[29–31] However, in actual biological systems, there are often significant differences in the coupling strengths and connection methods among neurons.[32–34] This coupling di-

[†]Corresponding author. E-mail: lululu@cug.edu.cn

© 2026 Chinese Physical Society and IOP Publishing Ltd. All rights, including for text and data mining, AI training, and similar technologies, are reserved.

versity may have a profound impact on the functions of neuronal networks. For example, Liang et al. studied the complementary role of positive and negative couplings in signal amplification and revealed the influence of coupling types on the system response.[35,36] Liu and Liang explored the influence of coupling diversity on globally coupled bistable oscillators and found that appropriate coupling diversity can enhance the system's response to weak signals.[37]

We extend the research on signal detection to a more realistic hybrid weighted positive and negative coupling FHN model and study how the coupling diversity of this model affects the collective response of the globally coupled bistable oscillator system to weak signals. Through numerical simulations and analytical calculations, we find that appropriate coupling diversity can lead to the splitting of the system dynamics and the generation of three oscillation clusters, thereby enhancing the collective response of the system to external weak signals. This indicates that coupling diversity may play a role similar to that of noise in signal detection.

2. Model and method

The FitzHugh–Nagumo (FHN) model acts as a mathematical depiction of neuronal dynamic behavior.[18,19] We analyze a system consisting of N globally coupled bistable oscillators that possess heterogeneity parameters.[28] The dynamics of this system are described as follows:

$$\begin{aligned}\varepsilon\frac{\mathrm{d}x_i}{\mathrm{d}t} &= x_i(1-x_i)(x_i-a)-y_i+\frac{c_i}{N}\sum_{j=1}^{N}(x_j-x_i)\\ &\quad +A\sin(\omega t),\quad i=1,2,\ldots,N,\\ \frac{\mathrm{d}y_i}{\mathrm{d}t} &= bx_i-y_i-d,\end{aligned}\tag{1}$$

where $i=1,2,\ldots,N$ denotes the number of neurons. The variable x_i, which represents the membrane potential of neuron i, is a fast variable, while y_i represents the slower recovery variable. To distinguish between fast and slow variables, the parameter ε is set to 0.01. The coupling strength c_i represents the coupling strength of oscillator i, which can be either positive or negative, arising from the neural networks of excitatory and inhibitory neurons.[39] When c_i is positive, oscillator i acts in a strongly attractive (excitatory) manner, tending to align closely with all the other oscillators. Conversely, when c_i is negative, it denotes a strongly repulsive (inhibitory) oscillator that tends to keep a considerable distance from its neighbors. For simplicity, we assume the coupling strength follows a Gaussian distribution with mean c_0 and variance $\langle(c_i-c_0)(c_j-c_0)\rangle=\delta_{ij}\sigma^2$, where the level of coupling diversity is controlled by the standard deviation σ. Thus the interactions between oscillator pairs become asymmetric and vary from one oscillator to another when $\sigma\neq 0$. $I=A\sin(\omega t)$ is defined as the external signal, where A and ω signify the amplitude and angular frequency, respectively. When $c_i=0$ and $I=0$, a single FHN neuron is bistable with stable fixed points at $(0.89,0.04)$ and $(0.11,-0.04)$.

To simulate a weak signal, we set $A=0.01$ and $\omega=\pi/50$, which ensures that the signal is subthreshold (at this frequency, the critical amplitude for input neuron spiking is $A_{\mathrm{th}}=0.017$[37]). Under this signal, each input neuron oscillator cannot switch between its two wells at $c_i=0$. The remaining parameters of the bistable neuron system are set as follows: $N=1000$, $a=0.5$, $b=0.1$, and $d=0.05$.[28]

In order to characterize the system's response to an external signal, the spectral amplification factor η is employed, which is formally defined as[27,38]

$$\eta=\left|\frac{2}{nAT}\int_0^{nT}X_i(t)\,\mathrm{e}^{\mathrm{i}\omega t}\,\mathrm{d}t\right|,\tag{2}$$

where the parameter T denotes the period of the external weak periodic signal, defining the fundamental time scale of the input signal to which the system responds. The parameter nT represents the total time window over which the system's response is measured and integrated, determining the temporal span of the time-series data used in the analysis. The parameter N specifies the total number of oscillators in the globally coupled network; in this study, N is set to 1000, representing the number of individual units whose collective dynamics govern the overall behavior of the network. $X_i(t)=N^{-1}\sum_{i=1}^{N}x_i(t)$ represents the average activity dynamics of the system, while A and ω represent the amplitude and angular frequency of the external signal, respectively.

3. Results and discussion

3.1. Numerical simulations

First, we investigated the signal amplification response of the two-dimensional fully coupled bistable system when the coupling strength follows a Gaussian distribution, specifically the dependence of the spectral amplification coefficient η on the mean c_0 and standard deviation σ of the diversity parameter. As shown in Fig. 1, significant signal amplification primarily occurs when the mean c_0 exceeds zero, and only weak signal responses are observed when the mean is negative. Moreover, as the mean increases, the optimal signal amplification response also gradually increases. For a fixed c_0, as the standard deviation σ of diversity increases, the spectral amplification coefficient η exhibits a bell-shaped trend. This indicates that under conditions of moderate diversity (moderate σ), the weak signal amplification effect is more likely to be induced. Additionally, under different mean conditions, as the standard deviation increases to a certain level, the signal amplification effect gradually decays to the initial signal response level. Therefore, it can be inferred that the diversity of

the coupling strength distribution can significantly impact the signal response of the proposed two-dimensional fully coupled bistable system, and this impact is controlled by both the mean and standard deviation of the diversity parameters.

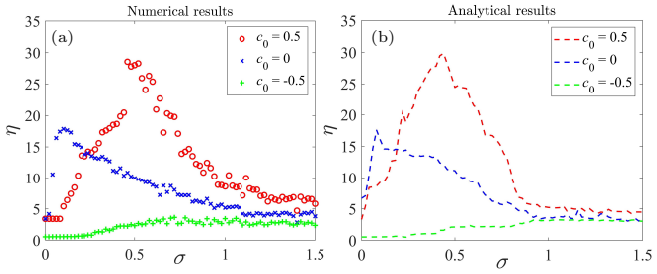


Fig. 1. The relationship between η and σ for fixed values of c_0 $(-0.5, 0, 0.5)$. (a) Numerical results, (b) analytical results.

Subsequently, experiments were implemented to verify the previously mentioned hypothesis and to elucidate the underlying causes. Based on Eq. (1) and the existing findings, we have systematically investigated the relationships between η and c_0, as well as between η and σ. The variation of η with σ is depicted in Fig. 2(a). As shown in Fig. 2(a), at intermediate mean values ($c_0 = 0.5$), the spectral amplification coefficient η is predominantly within the range $0 < \eta < 30$. When $\sigma > 0$, η increases rapidly as the disparity in the distribution grows, peaking at $\sigma \approx 0.5$. Beyond $\sigma = 0.5$, η drops sharply, making signal amplification unattainable. To gain a deeper understanding of this phenomenon, we simulated the temporal response of the neuronal time series. We set the average coupling strength $c_0 = 0.5$, and first investigated the scenario of uniform coupling strength where $\sigma = 0$. Numerical simulations reveal that under these conditions, the system achieves complete synchronization, with small-amplitude oscillations occurring around $x^* = 0.89$ (Fig. 2(b)). However, when $\sigma = 0.3$, the coupling strength exhibits a distribution, with a small fraction becoming negative. As a result, oscillators with negative coupling strength tend to repel other oscillators. Consequently, the synchronized cluster that existed at $\sigma = 0$ bifurcates into two distinct oscillation clusters. The oscillators in the second cluster exhibit minor fluctuations centered around $x^* = 0.11$ (Fig. 2(c)). As σ rises to 0.5, an increasing number of oscillators exhibit repulsive behavior, prompting the system to evolve into three distinct oscillation clusters. While the first two clusters oscillate around $x^* = 0.89$ and $x^* = 0.11$, the newly emerged third cluster alternates between these two states, resulting in a larger-amplitude oscillation centered around $x^* = 0.465$ (Fig. 2(d)). However, if σ continues to increase, the synchronization among the three clusters deteriorates (Fig. 2(e)).

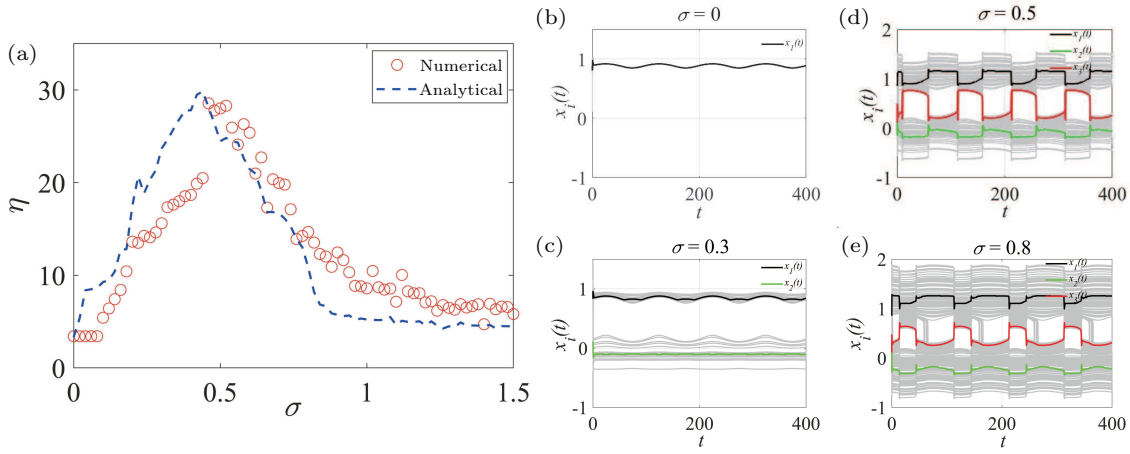


Fig. 2. (a) The signal amplification factor η of Eq. (1) as a function of σ at $c_0 = 0.5$. The blue solid line illustrates the theoretical results of Eqs. (12) and (20), whereas the red circles represent the numerical results. The corresponding time series x_i of Eq. (1) for $c_0 = 0.5$ with (b) $\sigma = 0$, (c) $\sigma = 0.3$, (d) $\sigma = 0.5$, and (e) $\sigma = 0.8$. In the figure, the black, green, and red lines represent the time-dependent evolution curves of the dynamic averages of the first, second, and third clusters of neurons, respectively.

To quantify the emergence of oscillation clusters, we classify oscillator i as belonging to the k_{th} cluster using the following criterion:

$$k = \begin{cases} 1, & \text{if } \min x_i(t) > 0.465, \\ 2, & \text{if } \max x_i(t) < 0.465, \\ 3, & \text{else.} \end{cases} \tag{3}$$

Let N_k represent the size of the k_{th} cluster. Figure 3(a) illustrates how N_k varies with σ when $c_0 = 0.5$. It is observed that N_1 gradually decreases while N_2 gradually increases until $\sigma_c \approx 0.4$, with $N_1 + N_2 = N$ maintained. Beyond this point, as σ increases further, N_1 drops sharply and converges toward N_2 until $N_1 \approx N_2$. In contrast, N_3 remains zero until $\sigma_c \approx 0.4$ and then exhibits a bell-shaped curve with respect to σ. To further investigate the impact of the mean coupling strength on cluster size, we examine cases with $c_0 = 0$ and $c_0 = -0.5$. In these scenarios, the oscillators cannot achieve synchronization at $\sigma = 0$ due to random initial conditions and instead split into two clusters of roughly equal size $(N_1 \approx N_2)$ (see Figs. 3(b) and 3(c)). As σ increases, N_3 begins to rise steadily, starting from $\sigma_c \approx 0$ when $c_0 = 0$ and from $\sigma_c \approx 0.4$ when $c_0 = -0.5$.

These findings demonstrate that a sufficient degree of coupling heterogeneity is essential for the emergence of three distinct oscillation clusters. Furthermore, an optimal level of coupling diversity enables the third cluster to exhibit a more significant oscillation amplitude, thereby exerting a dominant influence on the system's dynamics.

To more intuitively visualize the signal amplification regions, Fig. 4 illustrates the dependence of the spectral amplification factor η on σ for $c_0 = 0.5$, $c_0 = 0$, and $c_0 = -0.5$. The spectral amplification factor η remains constant when σ is below the critical value σ_c, increases significantly beyond this point, and eventually decreases when σ exceeds an optimal value $\sigma_0 \approx 0.5$. Collectively, these observations indicate that the spectral amplification factor exhibits a resonance phenomenon driven by the diversity of coupling strengths. This resonance effect is consistently observed for various values of c_0. As depicted in Fig. 4, the resonance effect becomes more pronounced with increasing c_0. Moreover, both the threshold σ_c and the optimal σ_0 increase progressively with c_0. Based on these results, we conclude that neither purely attractive interactions ($c_0 > 0$ and $\sigma = 0$) nor purely repulsive interactions ($c_0 < 0$ and $\sigma = 0$) are conducive to weak signal detection. In contrast, heterogeneous interactions that incorporate both attractive and repulsive coupling ($\sigma \neq 0$) significantly enhance signal detection.

First, we explain the mechanisms underlying two phenomena observed when $c_0 = 0.5$: (i) the division of oscillator dynamics in the system into multiple clusters, and (ii) the emergence of large-amplitude oscillations in the third cluster. This explanation is based on examining the relationship between the coupling strength c_i and the corresponding initial condition $x_i(0)$, as depicted in Fig. 5.

When σ is small ($\sigma = 0.3$), most oscillators exhibit positive coupling strengths ($c_i > 0$), while a small subset within the first cluster possesses negative coupling strengths ($c_i < 0$), as indicated by the black vertical lines in Fig. 5(a). There are two primary reasons why oscillators with negative coupling strengths ultimately join the first cluster: (i) their more positive initial conditions $x_i(0)$ facilitate synchronization with other oscillators in the potential well centered around $x^* = 0.89$; (ii) the attractive interactions from other oscillators outweigh their own repulsive effects. Conversely, in the second cluster, most oscillators have negative coupling strengths, with only a few exhibiting positive coupling strengths (Fig. 5(a)). Due to their inherent repulsive interactions and relatively smaller initial conditions [$x_i(0) = 0.11$], these oscillators collectively converge, thereby forming the second cluster localized around $x^* = 0.11$.

At the optimal coupling parameter $\sigma_0 = 0.5$, nearly all oscillators in the first and second clusters exhibit negative coupling strengths, whereas oscillators in the third cluster possess positive coupling strengths (Fig. 5(b)). The third cluster migrates cyclically: when approaching the first cluster, it is more strongly attracted by the second cluster ($|x_2 - x_3| > |x_1 - x_3|$) and moves downward; when approaching the second cluster, it is more strongly attracted by the first cluster ($|x_1 - x_3| > |x_2 - x_3|$) and moves upward. This cyclic motion provides the mechanism by which coupling diversity induces large-amplitude oscillations and enhances the system response to weak external signals.

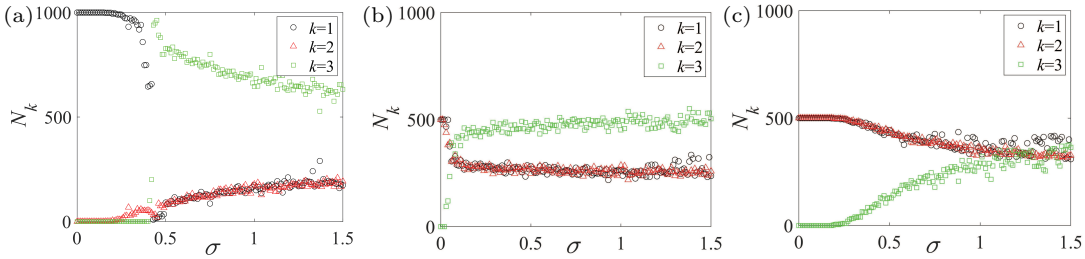


Fig. 3. The cluster size N_k versus σ for different values of c_0. (a) $c_0 = 0.5$, (b) $c_0 = 0$, (c) $c_0 = -0.5$.

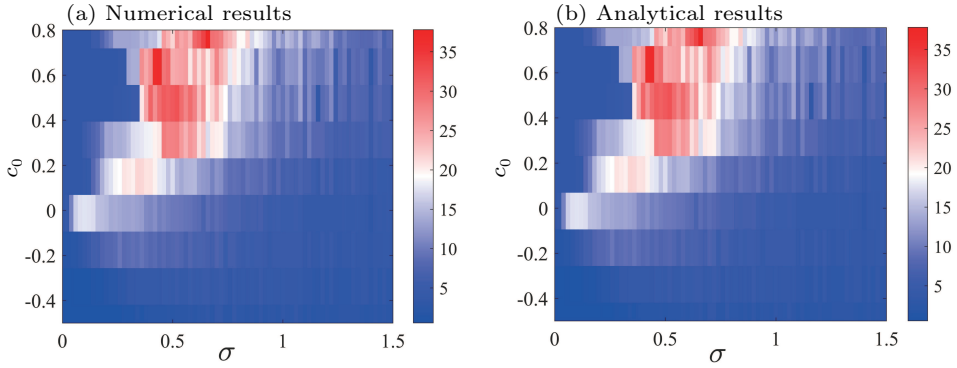


Fig. 4. The heatmap of the spectral amplification factor η versus σ and c_0. (a) Numerical results, (b) analytical results.

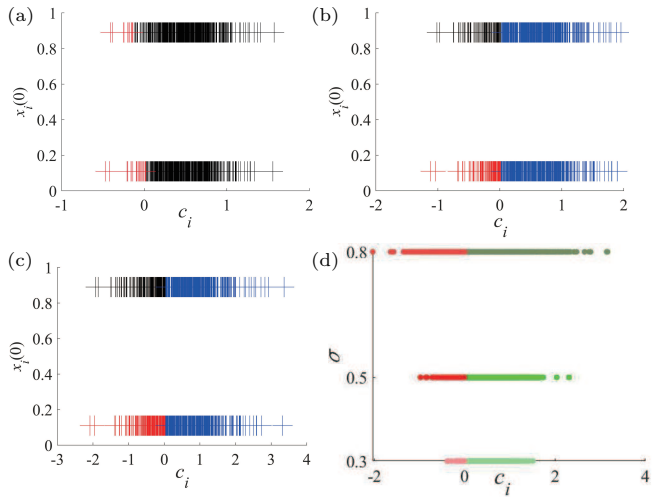


Fig. 5. Relationship between the coupling strength c_i and the initial condition $x_i(0)$ for each cluster at $c_0 = 0.5$ with (a) $\sigma = 0.3$, (b) $\sigma = 0.5$, and (c) $\sigma = 0.8$. The black, red, and blue vertical lines represent oscillators belonging to the first, second, and third clusters, respectively. Each panel shows a scatter plot of c_i for the given σ values.

Finally, when σ reaches 0.8, the significant dispersion in c_i enhances the system's repulsive characteristics (Fig. 5(c)), reducing both the size and synchronization of the third cluster; this directly diminishes the system's oscillation enhancement capability. To clarify the mechanism of weak signal amplification in our model, we first refer to existing findings: coupling disorder can induce resonance and chaos–order transitions, and both resonance and weak chaos influence weak signal amplification.[37,40] Our results further specify how coupling diversity regulates this process through inter-cluster interactions.[37,40]

To further elucidate the mechanism by which coupling diversity induces signal amplification, we analyzed the probability distribution of c_i under different σ values when $c_0 = 0.5$ (Fig. 5(d)).

When the coupling diversity is low ($\sigma = 0.3$), the system's coupling strength distribution is relatively concentrated, and most oscillators exhibit positive coupling ($c_i > 0$). This simple interaction constrains the system's resonance frequencies, limiting its response to a narrow range of external signals. Moreover, the system fails to induce weak chaos due to insufficiently complex interactions. Consequently, the system cannot amplify specific signals via resonance nor broaden its response range through weak chaos, resulting in signal decay under small internal disturbances.

At the optimal coupling parameter ($\sigma = 0.5$), only the third cluster exhibits positive coupling. This configuration enables precise resonance with external frequencies through a balance of inter-cluster positive and negative coupling, maximizing oscillator coordination for efficient energy absorption and signal amplification. It also induces weak chaos, sensitizing the system to disturbances and sustaining resonance for signal propagation.

When the coupling diversity is excessive, the third cluster shrinks and synchronization diminishes. Excessive coupling dispersion disrupts resonance, causing energy dissipation, while strong repulsion intensifies chaos — driving the system from ordered weak chaos to disordered strong chaos. As a result, signals experience interference and attenuation, degrading amplification performance.

Furthermore, we analyzed the potential energy V under different values of σ. At $\sigma = 0.3$, the potential energy exhibits an M-shaped profile, consisting of a central potential well and two barriers. These barriers fluctuate periodically over time, whereas the central well remains unchanged (Fig. 6(a)). In this case, particles initially located in the central well cannot overcome the barriers. When σ increases to 0.5, the external signal becomes suprathreshold, causing the barriers to vanish and allowing particles to escape from the well (Fig. 6(b)). At $\sigma = 0.8$, the potential energy transitions from an M-shaped to a U-shaped profile, featuring a single barrier with a narrower width, leading to smaller oscillation amplitudes (Fig. 6(c)). These findings collectively confirm that a moderate level of coupling diversity is optimal for signal amplification.

Finally, to demonstrate the robustness of signal amplification at moderate diversity levels, we plot the spectral amplification coefficient as a function of coupling diversity for different system sizes in Fig. 7. The results show that the larger the system size, the higher the peak value of the spectral amplification coefficient, but all peaks occur at moderate diversity levels. This finding further confirms the universal optimization effect of moderate diversity on signal amplification.

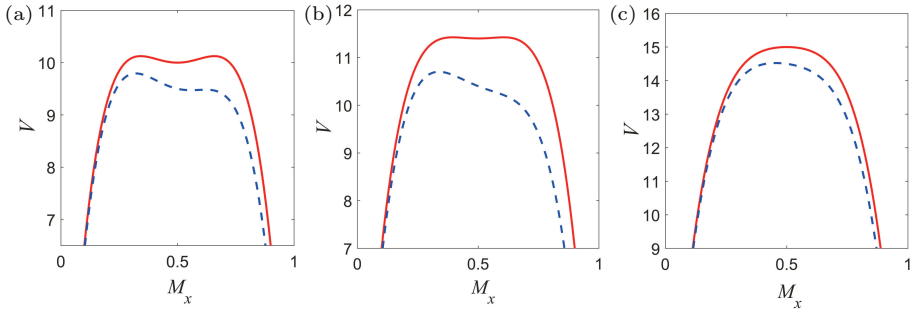


Fig. 6. Variation of the potential V for different coupling diversity σ. (a) $\sigma = 0.3$, (b) $\sigma = 0.5$, (c) $\sigma = 0.8$. The red solid line and blue dashed line denote the potential at $t = 0$ and $t = \pi/2\omega$, respectively.

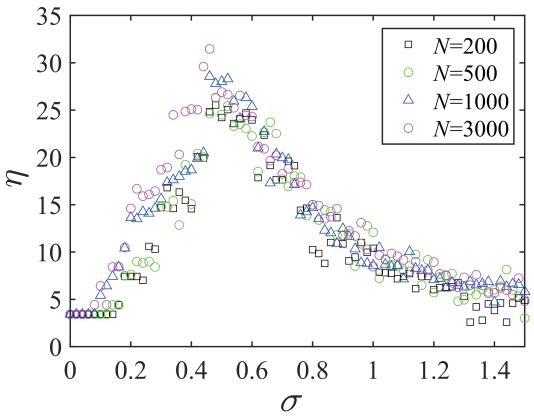


Fig. 7. Spectral amplification factor η versus coupling disorder σ for different system sizes.

3.2. Theoretical analysis

We now provide an analytical description of the aforementioned mechanism. When $0<\sigma<\sigma_c$, the system exhibits two oscillatory clusters. For simplicity, we assume that $N/2$ neurons oscillate around the stable fixed points $(0.89, 0.04)$ and $(0.11, 0.04)$, which are labeled as G_1 and G_2, respectively. The collective dynamics of clusters G_1 and G_2 are characterized by the variables X_1, Y_1 and X_2, Y_2. Accordingly, Eq. (1) can be rewritten as

$$\begin{aligned}
\varepsilon\frac{\mathrm{d}x_1}{\mathrm{d}t} &= x_1(1-x_1)(x_1-a)-y_1 \\
&\quad+\frac{c_i}{2}\sum_{j=1}^{2}(x_i-x_1)+A\sin(\omega t),\\
\frac{\mathrm{d}y_1}{\mathrm{d}t} &= bx_1-y_1-d,\\
\varepsilon\frac{\mathrm{d}x_2}{\mathrm{d}t} &= x_2(1-x_2)(x_2-a)-y_2 \\
&\quad+\frac{c_i}{2}\sum_{j=1}^{2}(x_i-x_2)+A\sin(\omega t),\\
\frac{\mathrm{d}y_2}{\mathrm{d}t} &= bx_2-y_2-d. \qquad (4)
\end{aligned}$$

We denote the mean activity and synchronization discrepancy of the two clusters as $M_x=(X_1+X_2)/2$, $M_y=(Y_1+Y_2)/2$, $D_x=(X_1-X_2)/2$, $D_y=(Y_1-Y_2)/2$. Then Eq. (4) can be rewritten as

$$\begin{cases}
\varepsilon\dfrac{\mathrm{d}M_x}{\mathrm{d}t} = -M_x^3+(a+1)M_x^2-(3D_x^2+a)M_x \\
\qquad\qquad -M_y+(a+1)D_x^2+A\sin(\omega t),\\
\dfrac{\mathrm{d}M_y}{\mathrm{d}t} = bM_x-M_y-c,\\
\varepsilon\dfrac{\mathrm{d}D_x}{\mathrm{d}t} = -D_x^3+[2(a+1)M_x-3M_x^2-a-c_i]D_x-D_y,\\
\dfrac{\mathrm{d}D_y}{\mathrm{d}t} = bD_x-D_y-c.
\end{cases} \qquad (5)$$

Employing the adiabatic elimination method, we assume that synchronization errors decay more rapidly than the average system dynamics, i.e., $\frac{\mathrm{d}D_x}{\mathrm{d}t}=0$, $\frac{\mathrm{d}D_y}{\mathrm{d}t}=0$. The equations then transform into

$$\begin{cases}
D_x^3=[2(a+1)M_x-3M_x^2-a-c_i]D_x-D_y,\\
bD_x=D_y-c.
\end{cases} \qquad (6)$$

This yields two solutions: $D_x=0$ (synchronous) and $D_x^2=2(a+1)M_x-3M_x^2-a-c_i-b$ (unsynchronized).

Here, we focus on the asynchronous case. Inserting the asynchronous solution into Eq. (5), we obtain

$$\begin{aligned}
\varepsilon\frac{\mathrm{d}M_x}{\mathrm{d}t} &= 8M_x^3-8(a+1)M_x^2+(2a^2+6a+3b+3c_i+2)M_x \\
&\quad -M_y-(a+1)(a+b+c_i)+A\sin(\omega t),\\
\frac{\mathrm{d}M_y}{\mathrm{d}t} &= bM_x-M_y-c. \qquad (7)
\end{aligned}$$

Next, employing the adiabatic elimination technique and setting $\varepsilon\frac{\mathrm{d}M_x}{\mathrm{d}t}=0$ in Eq. (7), we define

$$\begin{aligned}
f_1(M_x) &= 8M_x^3-8(a+1)M_x^2+(2a^2+6a+3b+3c_i+2)M_x \\
&\quad -(a+1)(a+b+c_i)=M_y-A\sin(\omega t). \qquad (8)
\end{aligned}$$

Thus, the evolution of M_y is governed by

$$\frac{\mathrm{d}M_y}{\mathrm{d}t}=bf_1^{-1}(M_y-A\sin(\omega t))-M_y-c, \qquad (9)$$

where f_1^{-1} denotes the inverse function of $f_1(M_x)$. Using the inverse proportionality approximation, we obtain

$$\begin{aligned}
M_x &= M_x^{(1)}+\sqrt{\frac{1+\omega^2}{[b-f_1'(M_x^{(1)})]^2+[\omega f_1'(M_x^{(1)})]^2}} \\
&\quad\times A\sin(\omega t+\varphi),\\
f_1'(M_x^{(1)}) &= 3c_i-0.2. \qquad (10)
\end{aligned}$$

Inserting Eq. (10) into Eq. (2) and integrating, we obtain the spectral amplification coefficient

$$\eta=\sqrt{\frac{1+\omega^2}{[b-f_1'(M_x^{(1)})]^2+[\omega f_1'(M_x^{(1)})]^2}}. \qquad (11)$$

When $\sigma>\sigma_c$, the system bifurcates into three distinct oscillation clusters. Denote the trajectory deviations in the third cluster as $\delta_j=x_j-x_3$ for $j\in N_3$. The mean coupling strength and deviation in the third cluster are defined as

$$\lambda_3=\frac{1}{N_3}\sum_{j=1}^{N_3}c_j,\quad \xi_j=c_j-\lambda_3. \qquad (12)$$

The average dynamics of the third cluster is

$$\frac{\mathrm{d}x_3}{\mathrm{d}t}=\frac{1}{N_3}\sum_{j=1}^{N_3}\frac{\mathrm{d}x_j}{\mathrm{d}t},\quad \frac{\mathrm{d}y_3}{\mathrm{d}t}=bx_3-y_3-d. \qquad (13)$$

Inserting Eq. (13) into Eq. (1) yields

$$\varepsilon\frac{\mathrm{d}x_3}{\mathrm{d}t}=\frac{1}{N_3}\sum_{j=1}^{N_3}\Big[x_j(1-x_j)(x_j-0.5)-y_3$$

$$+c_j(X-x_j)+A\sin(\omega t)\Big],$$
$$\frac{\mathrm{d}y_3}{\mathrm{d}t} = 0.1x_3 - y_3 - 0.05. \tag{14}$$

By expanding $x_j = x_3 + \delta_j$ and neglecting higher-order infinitesimals

$$\frac{1}{N_3}\sum_{j=1}^{N_3}(x_3+\delta_j)^3 \approx x_3^3,$$
$$\frac{1}{N_3}\sum_{j=1}^{N_3}(x_3+\delta_j)^2 \approx x_3^2,$$
$$\frac{1}{N_3}\sum_{j=1}^{N_3}c_j(x_3+\delta_j) \approx \lambda_3 x_3. \tag{15}$$

Substituting Eq. (15) into Eq. (14), we get

$$\varepsilon\frac{\mathrm{d}x_3}{\mathrm{d}t} = -\frac{x_3}{2} - x_3^3 + \frac{3x_3^2}{2} + \lambda_3 X - \lambda_3 x_3 - y_3 + A\sin(\omega t),$$
$$\frac{\mathrm{d}y_3}{\mathrm{d}t} = bx_3 - y_3 - d. \tag{16}$$

Assuming the third cluster dominates the global dynamics:

$$X = \frac{N_1x_1 + N_2x_2 + N_3x_3}{N} \approx \frac{N_3x_3}{N} \Rightarrow x_3 \approx \frac{NX}{N_3}. \tag{17}$$

Inserting Eq. (17) into Eq. (16) gives the global dynamics:

$$\varepsilon\frac{\mathrm{d}X}{\mathrm{d}t} = \Big[-\frac{1}{2} - \lambda_3\Big(1-\frac{N_3}{N}\Big)\Big]X - \Big(\frac{N}{N_3}\Big)^2 X^3 + \lambda_3 X + \frac{3N}{2N_3}X^2 - \frac{N_3}{N}y_3 + \frac{N_3}{N}A\sin(\omega t). \tag{18}$$

For Gaussian-distributed coupling strengths, the mean λ_3 is approximated by

$$\lambda_3 \approx \frac{c_0 + \sqrt{2}\sigma}{2}. \tag{19}$$

Finally, the simplified global dynamics becomes

$$\varepsilon\frac{\mathrm{d}x_3}{\mathrm{d}t} = \left[-\frac{1}{2} - \frac{c_0+\sqrt{2}\sigma}{2}\left(1-\frac{N_3}{N}\right)\right]X - \Big(\frac{N}{N_3}\Big)^2 X^3 + \lambda_3 X + \frac{3N}{2N_3}X^2 - \frac{N_3}{N}y_3 + \frac{N_3}{N}A\sin(\omega t),$$
$$\frac{\mathrm{d}y_3}{\mathrm{d}t} = 0.1x_3 - y_3 - 0.05. \tag{20}$$

Equation (20) describes a periodically driven bistable oscillator with parameters modulated by diversity. Using N_3 from Eq. (1) (see Fig. 2), numerical simulations of Eq. (20) produce $X(t)$, which, when substituted into Eq. (2), yields the spectral amplification factor η (see Fig. 3). Analytical predictions closely match numerical results, demonstrating that Eq. (20) accurately captures the primary dynamics of Eq. (1).

4. Conclusion

In this study, we investigated the impact of coupling diversity on signal transmission and amplification in a two-dimensional globally coupled bistable system. The coupling parameter c was assumed to follow a Gaussian distribution with mean c_0 and variance σ. Our results demonstrate that an optimal level of coupling diversity can significantly enhance the collective response of the system to weak external signals via a diversity-induced resonance mechanism. This finding highlights the crucial role of coupling diversity in modulating internal interactions and suggests new strategies for practical applications in signal processing and detection, including fault detection and biomedical signal analysis.

Numerical simulations and analytical calculations reveal that signal amplification depends sensitively on both the mean and variance of the coupling. With the mean fixed at 0.5, the spectral amplification coefficient η exhibits a bell-shaped dependence on σ, indicating that weak signals are most effectively amplified at intermediate levels of coupling diversity. Specifically, at the optimal diversity level near $\sigma \sim 0.5$, the system dynamics bifurcate into three distinct oscillation clusters: two clusters show small-amplitude oscillations, while one cluster exhibits large-amplitude oscillations. Remarkably, these two types of oscillation clusters induced by coupling diversity resemble the two characteristic responses of excitable neurons: small-amplitude subthreshold oscillations around the resting state, and sustained large-amplitude relaxation oscillations (resembling spiking). This bifurcation substantially enhances the system's sensitivity to weak external signals.

Our work extends the investigation of coupling diversity from one-dimensional to two-dimensional bistable systems, providing a more comprehensive perspective on signal amplification mechanisms in complex networks. The results indicate that heterogeneity in coupling — by introducing asymmetric and diverse interactions among oscillators — plays a vital role in enhancing the detection and transmission of weak signals.

A primary limitation of this study is the reliance on the FHN model, which provides a simplified representation of neural dynamics. Future research should explore the effects of coupling diversity in more realistic neural network models that incorporate both excitatory and inhibitory interactions.

Acknowledgments

This work was supported by the National Natural Science Foundation of China (Grant No. 12305054), the China Scholarship Council (Grant No. 202306410194), and the Guangdong Provincial Key Laboratory of Mathematical and Neural Dynamical Systems.

References

[1] Kobiolka J, Habermann J and Yamakou M E 2025 *Nonlinear Dyn.* **113** 10989
[2] Lebal A, Moussaoui A and Rezgui A 2023 *Multimed. Tools Appl.* **82** 17391
[3] Andersen J V, Schousboe A and Verkhratsky A 2022 *Prog. Neurobiol.* **217** 102331
[4] Wang Y, Bernat S and Vinogradov A 2024 *Expert Syst. Appl.* **258** 124832
[5] He Y, Qiao Z, Xie B, *et al.* 2024 *Chaos Solitons Fractals* **182** 114749
[6] Yun X, Zhang X, Shang G, *et al.* 2024 *Phys. Scr.* **99** 085244
[7] Liang X and Liu Z 2016 *Sci. China Technol. Sci.* **59** 376
[8] Shubita R R, Alsadeh A S and Khater I M 2023 *IEEE Access* **11** 6665
[9] Hänggi P 2002 *ChemPhysChem* **3** 285
[10] Dai S Q, Lu L L, Wei Z C, Zhu Y and Yi M 2022 *Chaos Solitons Fractals* **164** 112762
[11] Wang Z Q, Xu Y and Yang H 2016 *Sci. China Technol. Sci.* **59** 371
[12] Xu Y, Li J, Feng J, *et al.* 2013 *Eur. Phys. J. B* **86** 1
[13] Li D, Cui X and Yang Y 2018 *Neurocomputing* **287** 52
[14] McDonnell M D and Ward L M 2011 *Nat. Rev. Neurosci.* **12** 415
[15] Jiao S, Gao R, Xue Q, *et al.* 2023 *Chin. Phys. B* **32** 050202
[16] Yu D, Lu L, Wang G, *et al.* 2021 *Chaos Solitons Fractals* **147** 111000
[17] Valenti D, Augello G and Spagnolo B 2008 *Eur. Phys. J. B* **65** 443
[18] Zhou S, Huang G, Zhu R, *et al.* 2024 *Opt. Laser Technol.* **175** 110736
[19] Aqil M, Hong K S and Jeong M Y 2012 *Commun. Nonlinear Sci. Numer. Simul.* **17** 1615
[20] Zhang X, Min F, Dou Y, *et al.* 2023 *Chaos Solitons Fractals* **170** 113415
[21] Guo L, Zhao Q, Wu Y, *et al.* 2022 *Appl. Soft Comput.* **130** 109645
[22] Kondo T, Liu Z and Munakata T 2010 *Phys. Rev. E* **81** 041115
[23] Li T, Wu Y, Yang L, *et al.* 2022 *Physica A* **606** 128069
[24] Yilmaz E, Baysal V and Ozer M 2015 *Phys. Lett. A* **379** 1594
[25] Liu Z 2011 *Chin. Sci. Bull.* **56** 3623
[26] Ge Y and Liang X M 2020 *Commun. Theor. Phys.* **72** 055601
[27] Scialla S, Loppini A, Patriarca M, *et al.* 2021 *Phys. Rev. E* **103** 052211
[28] Wu Y, Wu L, Zhu Y, *et al.* 2024 *Chaos Solitons Fractals* **181** 114566
[29] Yu D, Zhou X, Wang G, *et al.* 2022 *Cogn. Neurodyn.* **16** 887
[30] Popovych O V, Yanchuk S and Tass P A 2011 *Phys. Rev. Lett.* **107** 228102
[31] Zhang X, Zhang C and Zhang Y 2024 *Comput. Math. Appl.* **157** 92
[32] Ning L and Liu T 2023 *Phys. Scr.* **98** 015210
[33] Liu C, Wang C Y, Wu Z X, *et al.* 2022 *Chaos* **32** 103101
[34] Gassel M, Glatt E and Kaiser F 2007 *Phys. Rev. E* **76** 016203
[35] Liang X and Zhao L 2012 *Neural Netw.* **35** 40
[36] Liang X, Zhang X and Zhao L 2020 *Chaos* **30**
[37] Liu C and Liang X 2019 *Phys. Rev. E* **100** 032206
[38] Qin B and Ning L 2025 *Phys. Scr.* **100** 075209
[39] Acebrón J A, Lozano S and Arenas A 2007 *Phys. Rev. Lett.* **99** 128701
[40] Liu C, Wu Z X and Guan J Y 2024 *Phys. Rev. Res.* **6** L042019